# Study of the transport and magnetic properties of substituted $Ba(Fe_{1-x}Ni_x)_2(Se_{1-y}Te_y)_3$

W. G. Zheng,[1,2,3] V. Balédent,[3] Y. Oubaid,[3] P. Auban-Senzier,[3] C. Colin,[4] F. Damay,[5] C. Pasquier,[3] A. Forget,[6] D. Colson,[6] J. P. Xu,[1,2] W. Yin,[1,2] P. Miao,[1,2,*] and P. Foury-Leylekian[3,†]

[1]*Institute of High Energy Physics Chinese Academy of Sciences, Beijing, 100049, People's Republic of China*
[2]*Spallation Neutron Source Science Center, Dongguan, 523803, People's Republic of China*
[3]*Université Paris-Saclay, CNRS, Laboratoire de Physique des Solides, 91405, Orsay, France*
[4]*Institut Néel, Université Grenoble Alpes, CNRS, Grenoble, F-38042, France*
[5]*Laboratoire Léon Brillouin,CEA-CNRS UMR12 91191 Gif-sur-Yvette Cedex, France*
[6]*SPEC, CEA, CNRS-UMR3680, Université Paris-Saclay, Gif-sur-Yvette Cedex 91191, France*

(Received 7 January 2024; revised 6 March 2024; accepted 25 April 2024; published 13 May 2024)

The magnetic order in $BaFe_2Se_3$, an iron-based spin ladder that is superconducting under pressure, is intensely studied due to the intimate relation between magnetism and superconductivity. In the present paper, we have performed a comprehensive study of structural, magnetic, and electronic properties on $Ba(Fe_{1-x}Ni_x)_2Se_3$ ($0 \leqslant x \leqslant 0.2$) and $BaFe_2(Se_{1-y}Te_y)_3$ ($0 \leqslant y \leqslant 0.15$). Neutron powder diffraction measurements were performed on the Ni-doped sample up to $x = 0.1$ and $BaFe_2(Se_{0.85}Te_{0.15})_3$. Our results show that the block magnetic order remains as the ground state for $x \leqslant 0.05$ in $Ba(Fe_{1-x}Ni_x)_2Se_3$. Additionally, for $BaFe_2(Se_{0.85}Te_{0.15})_3$, the block magnetic structure is even more robust. As for the resistivity, it decreases with increasing Ni content while it barely changes with Te doping. The observed negligible change of the magnetic propagation wave vector as a function of Ni content seems to contradict the orbital selective Mott Phase proposed previously.

DOI: 10.1103/PhysRevB.109.184428

## I. INTRODUCTION

Superconductivity in iron-based compounds remains a topic of intense debate within the scientific community [1,2]. One of the complexities arises from the presence of several Fe $3d$ orbitals for which the effect of electronic correlations can be different [3]. This can give rise to remarkable properties, including phase coexistence and a rich phase diagram. Recently, the antiferromagnetic (AFM) iron spin ladders $BaFe_2X_3$ ($X$ = S, Se) in which superconductivity was observed under pressure were of great interest. The crystal structures of $BaFe_2X_3$ are shown in Figs. 1(a) and 1(b). These systems consist of two iron ladders in each unit cell, with each ladder made up of two iron chains. Their reduced dimensionality simplifies theoretical models and offers hope for a better understanding of the superconductivity mechanism. Interestingly, the selenium compound is also multiferroic at ambient pressure and high temperature ($T_N = 250$ K), which makes it potentially valuable for spintronic applications [4]. At room temperature, the structures of these systems are different: *Cmcm* symmetry for $BaFe_2S_3$ and *Pnma* for $BaFe_2Se_3$ [5]. From a magnetic point of view, the two systems also exhibit distinctions. $BaFe_2Se_3$ shows an unusual block-like Néel order with spins perpendicular to the ladder and a magnetic propagation wave vector $\vec{k} = (\frac{1}{2}, \frac{1}{2}, \frac{1}{2})$ [Fig. 1(c)], which establishes below 250 K [6]. On the other hand, $BaFe_2S_3$ displays a stripelike magnetic structure with spins along the rung of the ladder and $\vec{k} = (\frac{1}{2}, 0, \frac{1}{2})$ [Fig. 1(d)], which is stabilized below 120 K [7]. Remarkably, the ordered magnetic moment on the Fe sites in the Néel state is smaller than the theoretical one [6], indicating the coexistence of itinerant and localized electrons in an orbital selective Mott phase (OSMP) [8].

The question of phase competition or coexistence in these compounds is of particular interest. The relevant phase diagram parameters are pressure (external or chemical) and electron or hole doping. The effect of external pressure has already been extensively studied. Pressure not only induces a superconducting state above 10 GPa in both compounds but also leads to a common crystallographic and stripe magnetic structure [7,9]. Specifically, under pressure, $BaFe_2Se_3$ undergoes a structural transition from *Pm* to *Cmcm* and a magnetic transition from a blocklike order to a stripelike one [9]. The discovery of this universal stripe magnetic structure is fundamental, as it appears to be a precursor of the superconducting phase.

In the context of carrier doping (electrons or holes), the general expectation is that it would increase conductivity, leading to a progressive metalization, a prerequisite for superconductivity as observed in cuprates or pnictides [10]. However, literature on the Cs-substituted $Ba_{1-x}Cs_xFe_2Se_3$ compound shows the opposite [11,12]. There is no improvement in conductivity, with the result that the stripe magnetic phase is more robust than the block one. The presence of a mixed valence of Fe was put forward to explain the transport properties, although no charge order was observed [11]. Another study attempted to electron dope this compound by substituting Co at the Fe site [13]. They showed that conductivity does increase with increasing Co concentration, but without reaching metallicity.

The fate of the extra electrons therefore remains an open question. At high substitution rates, the disorder induced on

*Corresponding author: miaoping@ihep.ac.cn
†Corresponding author: pascale.foury@u-psud.f

 

the iron ladders would tend to provoke Mott-Anderson localization, as in the case of $BaFe_2As_2$ [14]. In addition, a high substitution rate also disrupts magnetism. From a theoretical point of view, OSMP-based models [8] propose that the block magnetic structure of $BaFe_2Se_3$ can be modified by electron doping via a change in the $2k_F$ filling of the delocalized band, $k_F$ being the Fermi wave vector. As a consequence, the magnetic propagation wave vector would be modified. To investigate the influence of electron doping on magnetic properties, we decided to study Ni substitutions directly on the spin ladder. A previous study with Co substituted at the Fe site showed only weak effects [13] and we expect stronger modifications of $2k_F$ for $Ba(Fe_{1-x}Ni_x)_2Se_3$ $(0 \leqslant x \leqslant 0.2)$ compounds, knowing that each Ni atom brings two more electrons.

The substitutions can also affect the structure: this is the so-called chemical pressure. For example, the effect of substituting selenium with sulfur causes a rigid shift in their respective pressure-temperature phase diagrams [7,15]: sulfur induces a positive chemical pressure. Interestingly, substituting with a larger atom can produce a negative pressure effect, which is expected to enhance electronic correlations. In the case of $BaFe_2Se_3$, this effect can further stabilize the multiferroic phase. To further study the pure effect of chemical pressure, we have investigated the transport and magnetic properties of isoelectronic $BaSe_2(Se_{1-y}Te_y)_3$ $(0 \leqslant x \leqslant 0.15)$ compounds. We expect a negative chemical pressure which could lead to a stronger electronic localization, the enhancement of the exchange interactions, and the optimization of the multiferroic character.

## II. EXPERIMENTAL DETAILS

Single crystalline $Ba(Fe_{1-x}Ni_x)_2Se_3$ $(0 \leqslant x \leqslant 0.2)$ and $BaFe_2(Se_{1-y}Te_y)_3$ $(0 \leqslant y \leqslant 0.15)$ samples were synthesized using the melt-growth method. The doping ranges are limited to $x \leqslant 0.2$ and $y \leqslant 0.15$, since highly doped samples exhibit reduced crystallization and increased impurity content. On the other hand, we aim to investigate the low doping region where the magnetic structure remains intact. Small pieces of Ba (99.9%), powders of Fe(Ni) (99.9%) and Se(Te) (99.999%) were carefully weighted and mixed according to the nominal stoichiometric compositions. The resulting mixture was placed in a carbon crucible and sealed in a quartz tube under an Ar gas pressure of 300 mbar. The quartz tube was heated to 1100 °C and held for 24 h and slowly cooled to 750 °C with a rate of 5 °C/h, and then cooled down to room temperature at 100 °C/h. This process leads to the formation of needlelike crystals with the size of dozens of millimeters, which agglomerate to form centimeter-sized pellets. Macroscopic magnetic properties were measured using a Quantum Design Magnetic Property Measurement System in various magnetic fields and temperatures. Temperature-dependent resistivity measurements were performed using a Quantum Design Physical Property Measurement System. The typical crystals used are elongated along the *b* axis. They are 2 to 3 mm in length (L) with a large dispersion for the section (S) leading to geometrical factors L/S between 20 and 300 $cm^{-1}$. A four-contact configuration was used with a dc current of maximum value 20 μA applied along the *b* axis.

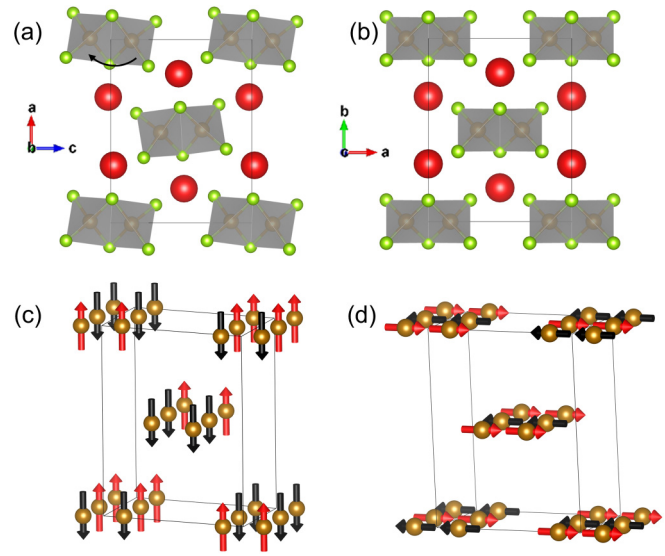


FIG. 1. (a), (c) Crystal structure and blocklike magnetic order of $BaFe_2Se_3$ in *Pnma* space group, respectively. (b), (d) Crystal structure and stripelike magnetic order of $BaFe_2S_3$ in *Cmcm* space group, respectively. The Fe, Se, and Ba atoms are shown with yellow, green, and red spheres. One should notice that the Fe ladders in *Pnma* structure display a tilting (indicated by the black arrow) while they are parallel to the *a* axis in *Cmcm*.

As for neutron powder diffraction (NPD) measurements, they were carried out on various beamlines, G4-1 of Laboratoire Léon Brillouin, D1B of Institut Laue-Langevin [16], Multi-Physics Instrument (MPI) of China Spallation Neutron Source [17], and SPICA of Japan Proton Accelerator Research Complex. The powder used in the NPD measurements is obtained by grinding the single crystals. All information concerning these diffractometers is summarized in Table 1 of the Supplemental Material [18]. The refinements of the obtained neutron diffractograms were performed by the FULLPROF suite [19]. One should note that $BaFe_2Se_3$ crystallizes in the *Pm* space group instead of the average structure of higher symmetry *Pnma* [20,21]. However, the slight difference between *Pm* and *Pnma* space groups is indistinguishable in our neutron powder diffraction as shown in Fig. 1 of the SM. To reduce the refined parameters, we used the *Pnma* space group to refine the powder data.

## III. RESULTS

### A. General characterization

We have synthesized $Ba(Fe_{1-x}Ni_x)_2Se_3$ compounds with $x = 0$, 0.005, 0.015, 0.04, 0.05, 0.1, 0.15, and 0.2, and $BaFe_2(Se_{1-y}Te_y)_3$ compounds with $y = 0.01$, 0.05, and 0.15. All samples have been carefully characterized via powder x-ray diffraction (after grinding the single crystals), energy dispersive x-ray spectroscopy (EDX), and magnetization measurements. Figure 2 presents the neutron diffraction patterns at 5 K together with Rietveld refinements for each Ni substitution. The obtained unit cell parameters and atomic positions are given in Tables 2 and 3 in the SM. The Rietveld refinements reveal that the main phase of each Ni-doped compound

TABLE I. Ni and Te concentration extracted from EDX measurements for each sample of this study and compared with the nominal stoichiometry. The $Fe_7Se_8$ fractions are obtained from the refinements of NPD patterns, with the error in parenthesis.

| Dopant | Ni | | | | | | | | Te | | |
|---|---|---|---|---|---|---|---|---|---|---|---|
| Nominal (%) | 0 | 0.5 | 1.5 | 4 | 5 | 10 | 15 | 20 | 1 | 5 | 15 |
| EDX value (%) | 0 | 0.5(0.1) | 1.7(0.1) | 4.5(0.3) | 5.1(0.2) | 9.8(0.5) | 17.0(0.4) | 18.6(0.3) | 1.2(0.2) | 4.9(0.3) | 15.1(1.2) |
| $Fe_7Se_8$ (%) | 0.62(0.29) | 1.57(0.23) | 0.36(0.26) | 3.92(0.21) | 4.59(0.17) | 1.26(0.15) | | | | | 1.06(0.20) |

consists of mainly the $BaFe_2Se_3$ phase and a few percent of $Fe_7Se_8$ impurities (see Fig. 2 and Table I). Although $Fe_7Se_8$ presents a magnetic reorientation at 125 K [22], its low concentration barely influences the NPD or charge transport characterizations.

EDX measurements with quantitative analysis on compositions were performed systematically on all the samples. Good homogeneity along the surface was confirmed. The actual concentrations of some Ni-doped samples show slight bias against the nominal value, as shown in Table I. There is no (Fe, Ni) deficiency while a slight deficiency in Se concentration was observed, which is ascribed to the volatility of Se.

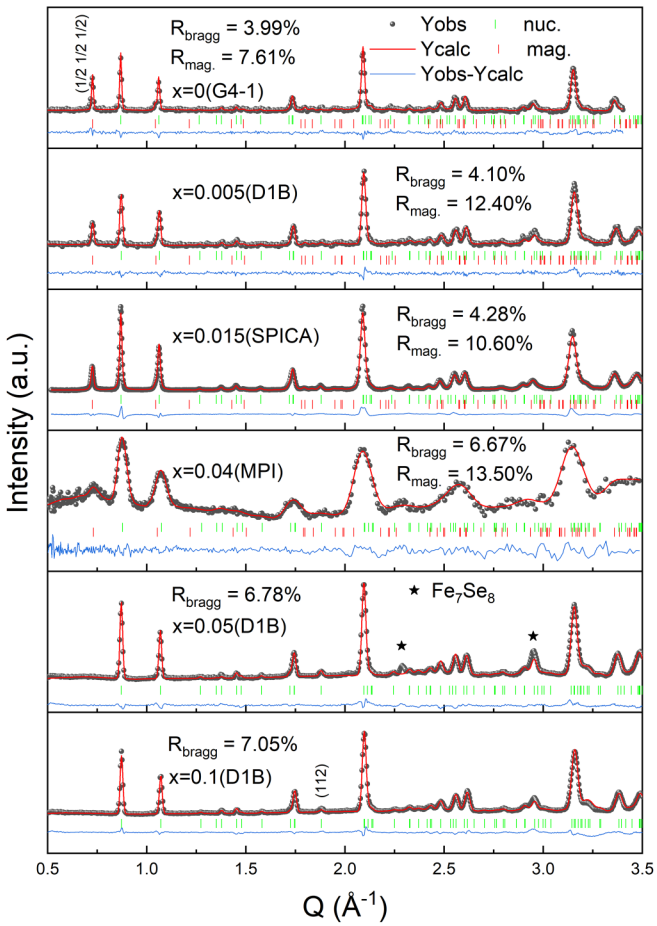


FIG. 2. (a) Neutron powder diffractograms and refinements for $Ba(Fe_{1-x}Ni_x)_2Se_3$ at 5 K. The diffractograms were collected at different beamlines as labeled. The green and red ticks indicate the nuclear and magnetic peaks, respectively. The peaks of $Fe_7Se_8$ impurity are marked with the stars. The (112) reflection peak, which is forbidden in the *Cmcm* space group, is also marked.

### B. Ni-doped compounds

#### 1. *Transport and magnetization measurements*

The temperature-dependent resistivities along the *b* axis for $Ba(Fe_{1-x}Ni_x)_2Se_3$ compounds are shown in Fig. 3(a). At room temperature, it decreases from 1.5 to 0.01 Ω cm, with *x* varying from 0 to 0.2 [Fig. 3(c)]. All compositions remain insulating despite the resistivity decreases for two orders of magnitude upon doping. This result is similar to what has been observed in Co-doped compounds [13], where Co doping also improves conductivity without

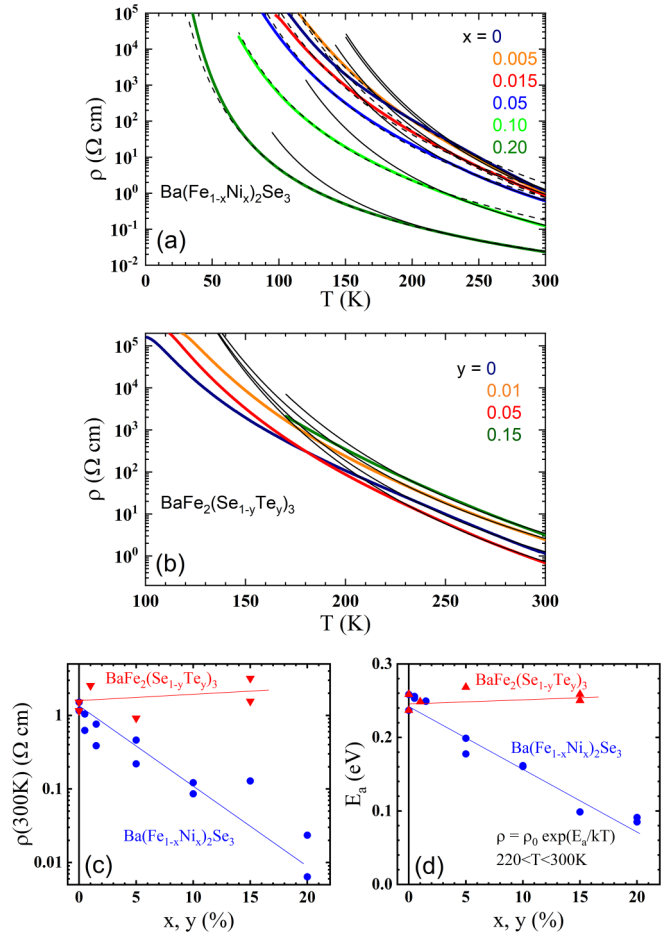


FIG. 3. (a), (b) Temperature dependence of electrical resistivity ($\rho$) for $Ba(Fe_{1-x}Ni_x)_2Se_3$ and $BaFe_2(Se_{1-y}Te_y)_3$, respectively. The continuous (dashed) black lines are the fittings with an activation (1D VRH) law. (c) Resistivity at 300 K, (d) activation energy determined in the high-temperature range (220–300 K) for $Ba(Fe_{1-x}Ni_x)_2Se_3$ and $BaFe_2(Se_{1-y}Te_y)_3$. Several compounds were measured on two specimens to ensure reliability. The red and blue lines are guides for the eyes.

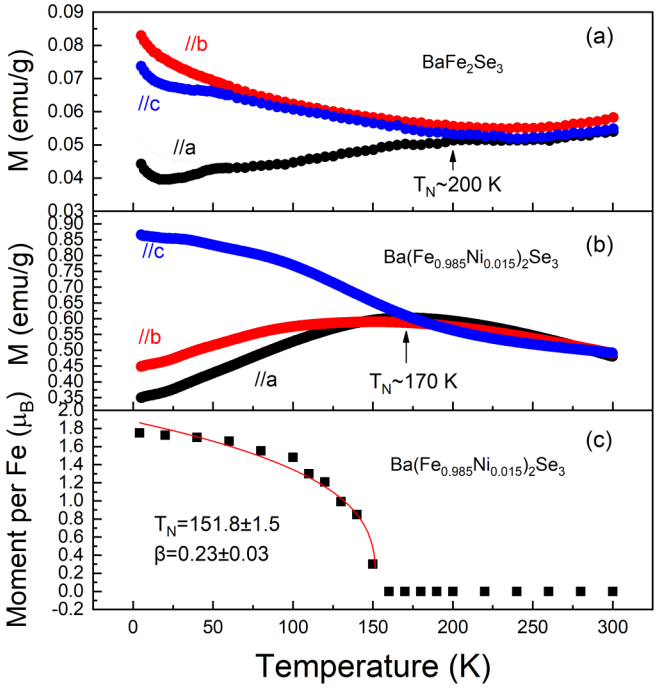


FIG. 4. (a) Temperature dependence of magnetization of $BaFe_2Se_3$ under 10 kOe. The bump around 50 K indicates a spin-glass-like transition which has been investigated in our previous study [26]. (b) Temperature dependence of magnetization of $Ba(Fe_{0.985}Ni_{0.015})_2Se_3$ under 10 kOe. (c) Temperature dependence of magnetic moment per Fe of $Ba(Fe_{0.985}Ni_{0.015})_2Se_3$ extracted from the NPD. The red line is the power-law fitting curve.

achieving metallization. By fitting experimental data in the high-temperature range (220–300 K) to the equation of $\rho = \rho_0 \exp[\frac{E_a}{kT}]$, the activation energy $E_a$ is obtained, which decreases from 0.24 to 0.09 eV, with $x$ varying from 0 to 0.2 [Fig. 3(d)]. In the low-temperature range (below 200 K), $\rho(T)$ curves are better described by the one-dimensional variable-range-hopping (VRH) model: $\rho = \rho_0^{1D} \exp[\frac{E_a^{1D}}{kT}]^{1/2}$. The resultant activation energy $E_a^{1D}$ decreases from 8 to 1 eV from $x = 0$ to 0.2 [Fig. 3(a)]. The low-dimensional character of $Ba(Fe_{1-x}Ni_x)_2Se_3$ at low temperature is similar with Co-doped $BaFe_2Se_3$ [13].

Magnetization as a function of temperature was measured in different crystal orientations, i.e., with a magnetic field perpendicular to the ladder ($a$ axis), along the ladder direction ($b$ axis), and the rung of the ladder ($c$ axis). Samples are cooled down in zero field and measured with an applied field of 10 kOe. Figures 4(a) and 4(b) show the results for $x = 0$ and $x = 0.015$, respectively. As we can see, a maximum of magnetization is visible on the curves along $a$ and $b$ for $Ba(Fe_{0.985}Ni_{0.015})_2Se_3$ while it is only observed along the $a$ axis for $BaFe_2Se_3$. This behavior indicates a change of magnetic easy axis from the $a$ axis to $(a, b)$ plane with Ni doping. Such a change of the single-ion magnetic anisotropy was observed for all Ni-doped samples with $0 < x < 0.05$. The Néel temperatures $T_N$ determined from magnetization measurements are represented in Fig. 5(a) as a function of $x$. Note that the reported $T_N$ for undoped $BaFe_2Se_3$ varies from 140 to 256 K [6,23–25], which is likely due to slight deviation from the ideal $BaFe_2Se_3$ stoichiometry [25].

#### *2. Neutron powder diffraction*

Figure 2 shows the neutron powder diffraction patterns at 5 K collected on $Ba(Fe_{1-x}Ni_x)_2Se_3$ ($0 \leqslant x \leqslant 0.1$). The broad peak of the MPI pattern is due to the intrinsic low Q-resolution of the low-angle detector bank from which the data were collected. As shown in Fig. 2, no signature of crystal structural transition has been identified in the diffractogram with Ni doping up to $x = 0.1$, suggesting the systems remain in the *Pnma* average space group. In the case of substituting S for Se, a structural transition from *Pnma* to *Cmcm* occurs at approximately 75% substitution [27]. But in $Ba(Fe_{1-x}Ni_x)_2Se_3$, the 112 reflection, which is forbidden in the *Cmcm* space group, is found in all doping levels. The unit cell parameters at 5 K were extracted from Rietveld refinement, and the relative differences to the undoped compound are plotted as a function of Ni doping in Fig. 5(c). The primary change occurs in the lattice constant $a$ (perpendicular to the Fe ladder), which decreases for nearly 1% at $x = 0.1$. The same behavior was observed in the Co substituted polymorphs [13]. This is ascribed to the chemical pressure effect since both Ni and Co have smaller atomic radii than Fe. Interestingly, a similar anisotropic evolution of the unit cell parameters is observed under hydrostatic pressure [Fig. 5(d)], where compression of $a$ is twice stronger than that in $b$ and $c$ [9,28]. The contraction of the lattice by substitution with Ni is comparable to what has been observed under pressure below a few gigapascals.

The $\frac{1}{2}\frac{1}{2}\frac{1}{2}$ reflection was observed at low temperatures for Ni doping up to $x = 0.05$ [Fig. 2], with a similar peak width to those of the nuclear reflections, indicating the long-range magnetic order. The magnetic intensities can be well described by Rietveld refinement using the block-model magnetic structure proposed for the undoped $BaFe_2Se_3$ [6]. The obtained moment per Fe for each Ni content at 5 K is shown in Fig. 5(b). By fitting the temperature dependence of the magnetic moment with the classical power-law function $m(T) = m_0(1 - \frac{T}{T_N})^{\beta}$, we could extract the Néel temperature. For example, Fig. 4(b) shows the temperature dependence of moment at $x = 0.015$, and the fitting gives a $T_N$ of $152 \pm 2$ K and a critical exponent $\beta$ of $0.23 \pm 0.03$. The obtained $T_N$ for each Ni content is displayed in Fig. 5(a), which is consistent with that derived from the magnetization measurements. As shown in Figs. 5(a) and 5(b), the long-range magnetic order is rapidly suppressed by Ni doping while for Co doping [13] it persists up to 10% doping. This indicates a stronger influence of Ni substitution on the stabilization of the magnetic order. This is explained by the two-electron difference between Ni and Fe, which induces a more significant perturbation of the spin chain than with Co, which differs by just one electron from Fe, as reported in parent compounds $BaFe_2As_2$ [29]. If these results tend to indicate that the substitution of Co and Ni leads to electron doping, the effective quantity of electrons and their fate in the electronic structure remain to be elucidated.

### C. $BaFe_2(Se_{1-y}Te_y)_3$

The temperature-dependent resistivities along the $b$ axis for $BaFe_2(Se_{1-y}Te_y)_3$ ($y = 0.01, 0.05$, and 0.15) are shown in Fig. 3(b). The room-temperature resistivity and activation energy of all the Te-substituted samples are very similar to

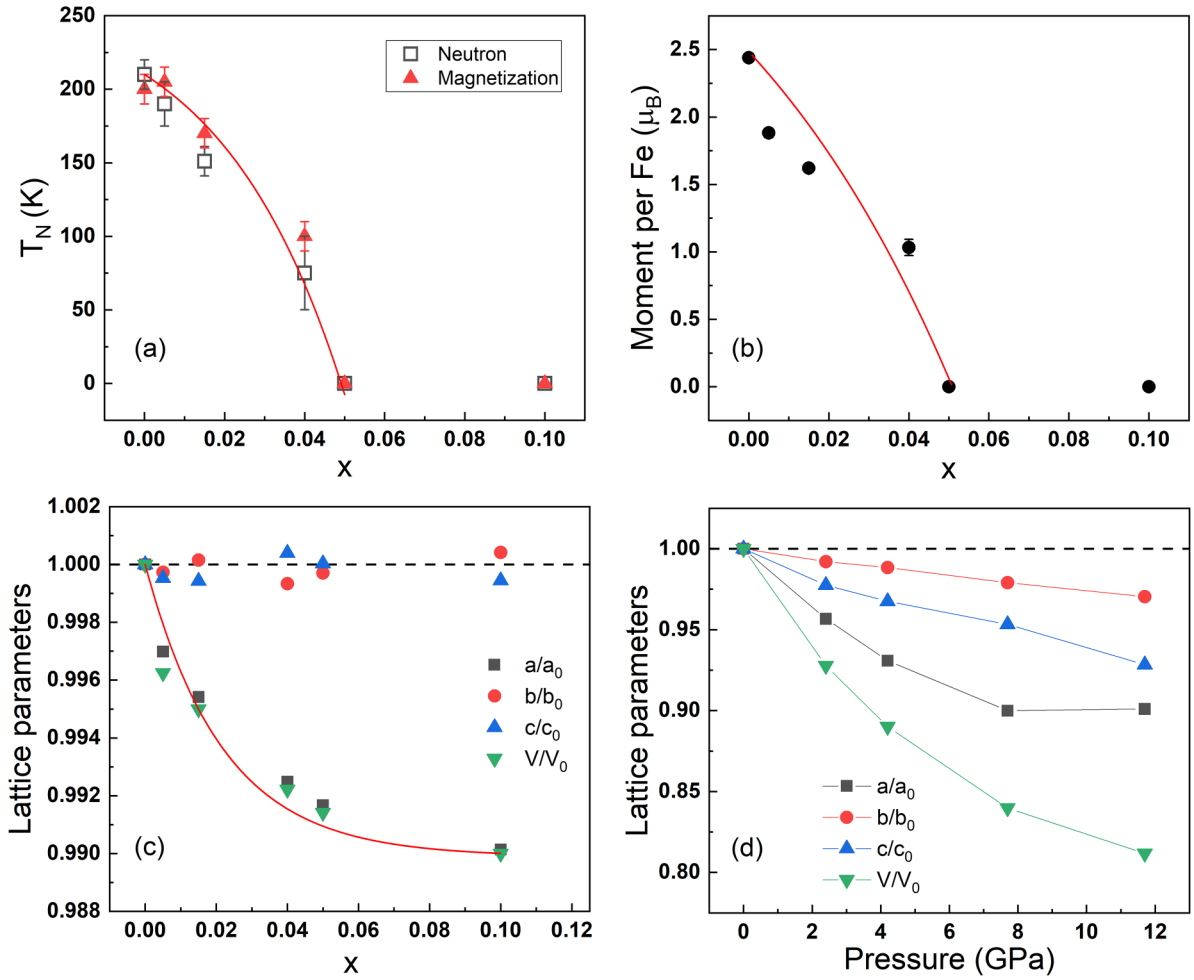


FIG. 5. (a) Néel temperature estimated from NPD and magnetization measurements, (b) magnetic moment at 5 K extracted from the refinement of the NPD pattern, (c) unit cell parameters as a function of $x$ for $Ba(Fe_{1-x}Ni_x)_2Se_3$. The red lines are guides for the eyes. (d) Unit cell parameters of $BaFe_2Se_3$ as a function of pressure based on our previous work [9].

those of the undoped compound [see in Figs. 3(c) and 3(d)], indicating that the transport properties are barely affected by Te substitution.

Magnetization and neutron diffraction measurements were carried out on $BaFe_2(Se_{0.85}Te_{0.15})_3$. A maximum of magnetization at around 200 K along the $a$ axis (perpendicular to the ladder) suggests an AFM transition [Fig. 6(b)]. The neutron powder diffraction experiment confirmed the presence of the magnetic reflection $\frac{1}{2}\frac{1}{2}\frac{1}{2}$ [Fig. 6(a)], which indicates that the blocklike magnetic order is maintained. In addition, the Rietveld refinement of the NPD data leads to a magnetic moment of $2.2\,\mu_B$ and lattice constants of $a = 12.02$ Å, $b = 5.41$ Å, and $c = 9.23$ Å at 5 K. More structural details are shown in Tables 2 and 3 of the SM. By fitting the temperature dependence of the magnetic moment, $T_N = 193.5 \pm 7$ K and the critical exponent $\beta = 0.21 \pm 0.07$ are derived as shown in Fig. 6(c). The $T_N$, $\beta$, and magnetic moment of $BaFe_2(Se_{0.85}Te_{0.15})_3$ are all very close to the ones in the undoped compound [9], indicating that Te doping does not modify the magnetic properties as well.

## IV. DISCUSSION AND CONCLUSION

The substitution of Se by Te has revealed that Te has little influence on the physical properties of these systems. Indeed, for the substitution as high as 15%, the negative chemical pressure effect is confirmed, with an expansion of 1.5% and 1.1% along the $a$ and $c$ axes, respectively, but surprisingly no change along the ladders ($b$ axis). In terms of transport and magnetic properties, neither the activation energy, nor the amplitude of the ordered moment, nor the $T_N$, nor the critical exponent are modified compared with the undoped compound. Further research is needed due to the limited Te-doped points in our current study.

On the other hand, our combined experiments involving diffraction and resistivity in $Ba(Fe_{1-x}Ni_x)_2Se_3$ have revealed a different effect of Ni substitution on Fe in terms of structure and transport properties. First, there is an observed increase in electrical conductivity with Ni concentration, reducing the gap by a factor of 3 between the undoped compound and $x = 0.2$. This result suggests effective electron doping, confirming what has been reported for Co substitution. However, in both cases, this substitution did not lead to metallization,

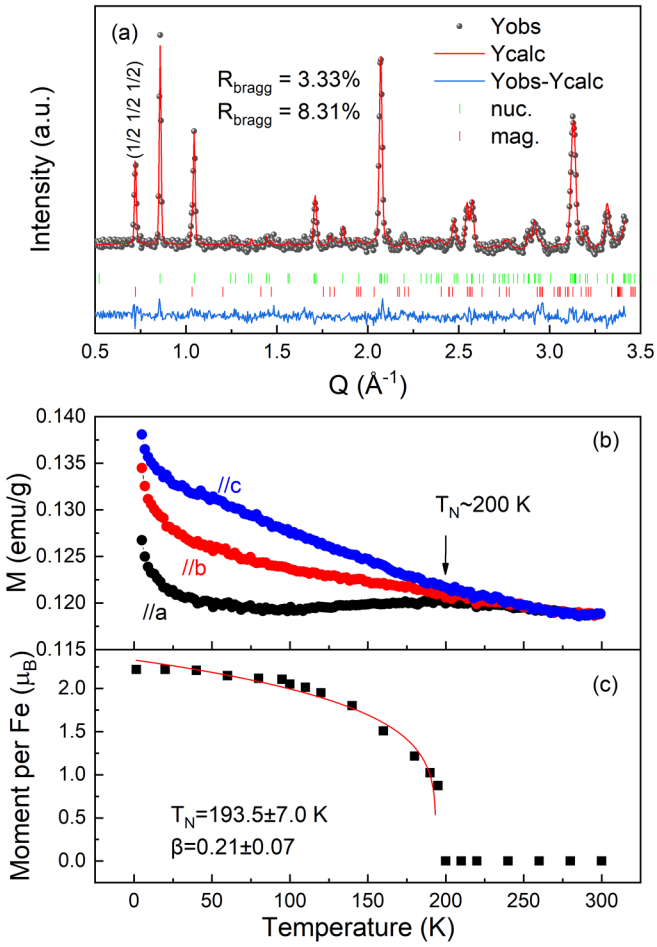


FIG. 6. (a) Neutron powder diffractogram at 5 K, (b) temperature dependence of magnetization under 10 kOe, (c) temperature dependence of magnetic moment per Fe extracted from the NPD for $BaFe_2(Se_{0.85}Te_{0.15})_3$. The red line is the power-law fitting curve.

and the system remains insulating. This effect may be associated with a disordering effect leading to Mott-Anderson localization at high enough concentrations [13]. As suggested in the literature, this increase in carrier density should modify the Fermi surface [13]. However, this intuition should be taken with caution. Indeed, in 2D pnictides, the authors of Ref. [14] showed no modification of the Fermi surface with doping while those of Ref. [30] obtained a filling of the band by Co doping. An OSMP-type phase could reconcile these two scenarios. It proposes the presence of two types of electrons: electrons localized by correlations on a half-filled band and itinerant electrons on the other band. According to Ref. [31], in the context of an OSMP phase, electron doping modifies $2k_F$ and leads to the stabilization of a block magnetic order of different shape and range from the order of the undoped $\pi/2$ block compound. Typically, for $x = 0.04$ (4%) Ni-doped compound, $Ba(Fe_{0.96}Ni_{0.04})_2Se_3$, Ni could yield 0.16 electrons to the conduction band [32]. This value is probably overestimated as the system remains insulating. However, a part of these electrons are active as the resistivity decreases. If these doping electrons all go into the iron bands, it would lead to an electron filling $n$ of 2.58 [33], using the notations from Ref. [31]. At such fillings, the system would theoretically present an incommensurate block order. Experimentally, this would be characterized by a change in propagation vector and/or accompanied by a broadening of magnetic reflections. Neither of these effects have been observed. Under Ni doping, our measurements show that the magnetic order remains identical at low doping. The propagation vector remains unchanged, and ordering takes place at a long range. There may be at least two main reasons for this contradiction: either the OSMP theory doesn't capture all the physics of the system or the extra electrons don't come into the iron bands. This second hypothesis is supported by experimental results on another iron superconductor $BaFe_2As_2$. Indeed, x-ray absorption spectroscopy measurements reveal that electron doping by Co substitution at the Fe site modifies not the electronic structure of the iron [34] but that of the ligand, in this case As [35]. A similar scenario may be at work in doped $BaFe_2Se_3$, where an additional injected electron may acquire a Se character. Further studies using angle-resolved photoemission, Hall effect, and x-ray absorption spectroscopy could shed further light on the effect of substitution and, in particular, on the fate of additional electrons in these compounds.

## ACKNOWLEDGMENTS

This work was financially supported by the China Postdoctoral Science Foundation (No. 2023M732031), the National Natural Science Foundation of China (NSFC) (No. 12005243), the Guangdong Basic and Applied Basic Research Foundation (No. 2022B1515120014, No. 2023B0303000003 and No. 2023B1515120060), ANR COCOM 20-CE30-0029, and the France 2030 program ANR-11-IDEX-0003 via Integrative Institute of Materials from Paris-Saclay University—2IM@UPSaclay. We acknowledge Songshan Lake Materials Laboratory for magnetometry and resistivity measurements and the MORPHEUS platform at the Laboratoire de Physique des Solides for sample alignment. We also thank the CRG-D1B and the 2FDN federation for the neutron experiments.

[1] G. R. Stewart, Superconductivity in iron compounds, Rev. Mod. Phys. **83**, 1589 (2011).

[2] P. Dai, J. Hu, and E. Dagotto, Magnetism and its microscopic origin in iron-based high-temperature superconductors, Nat. Phys. **8**, 709 (2012).

[3] Q. Si, R. Yu, and E. Abrahams, High-temperature superconductivity in iron pnictides and chalcogenides, Nat. Rev. Mater. **1**, 16017 (2016).

[4] S. Dong, J.-M. Liu, and E. Dagotto, $BaFe_2Se_3$: A high $T_C$ magnetic multiferroic with large ferrielectric polarization, Phys. Rev. Lett. **113**, 187204 (2014).

[5] H. Hong and H. Steinfink, The crystal chemistry of phases in the Ba Fe S and Se systems, J. Solid State Chem. **5**, 93 (1972).

[6] J. Caron, J. Neilson, D. Miller, A. Llobet, and T. McQueen, Iron displacements and magnetoelastic coupling in the

antiferromagnetic spin-ladder compound $BaFe_2Se_3$, Phys. Rev. B **84**, 180409(R) (2011).

[7] H. Takahashi, A. Sugimoto, Y. Nambu, T. Yamauchi, Y. Hirata, T. Kawakami, M. Avdeev, K. Matsubayashi, F. Du, C. Kawashima, H. Soeda, S. Nakano, Y. Uwatoko, Y. Ueda, T. J. Sato, and K. Ohgushi, Pressure-induced superconductivity in the iron-based ladder material $BaFe_2S_3$, Nat. Mater. **14**, 1008 (2015).

[8] J. Herbrych, N. Kaushal, A. Nocera, G. Alvarez, A. Moreo, and E. Dagotto, Spin dynamics of the block orbital-selective Mott phase, Nat. Commun. **9**, 3736 (2018).

[9] W.-G. Zheng, V. Balédent, C. V. Colin, F. Damay, J.-P. Rueff, A. Forget, D. Colson, and P. Foury-Leylekian, Universal stripe order as a precursor of the superconducting phase in pressurized $BaFe_2Se_3$ spin ladder, Commun. Phys. **5**, 183 (2022).

[10] A. Iyo, K. Kawashima, S. Ishida, H. Fujihisa, Y. Gotoh, H. Eisaki, and Y. Yoshida, Superconductivity on hole-doping side of $(La_{0.5-x}Na_{0.5+x})Fe_2As_2$, J. Am. Chem. Soc. **140**, 369 (2018).

[11] F. Du, K. Ohgushi, Y. Nambu, T. Kawakami, M. Avdeev, Y. Hirata, Y. Watanabe, T. J. Sato, and Y. Ueda, Stripelike magnetism in a mixed-valence insulating state of the Fe-based ladder compound $CsFe_2Se_3$, Phys. Rev. B **85**, 214436 (2012).

[12] T. Hawai, Y. Nambu, K. Ohgushi, F. Du, Y. Hirata, M. Avdeev, Y. Uwatoko, Y. Sekine, H. Fukazawa, J. Ma, S. Chi, Y. Ueda, H. Yoshizawa, and T. J. Sato, Temperature and composition phase diagram in the iron-based ladder compounds $Ba_{1-x}Cs_xFe_2Se_3$, Phys. Rev. B **91**, 184416 (2015).

[13] F. Du, Y. Hirata, K. Matsubayashi, Y. Uwatoko, Y. Ueda, and K. Ohgushi, Doping-and pressure-induced change of electrical and magnetic properties in the Fe-based spin-ladder compound $BaFe_2Se_3$, Phys. Rev. B **90**, 085143 (2014).

[14] H. Wadati, I. Elfimov, and G. A. Sawatzky, Where are the extra *d* electrons in transition-metal-substituted iron pnictides? Phys. Rev. Lett. **105**, 157004 (2010).

[15] J. Ying, H. Lei, C. Petrovic, Y. Xiao, and V. V. Struzhkin, Interplay of magnetism and superconductivity in the compressed Fe-ladder compound $BaFe_2Se_3$, Phys. Rev. B **95**, 241109(R) (2017).

[16] W. Zheng, V. Baledent, Claire V. Colin, and P. Foury-Leylekian, Doping induced change of magnetic structure in $BaFe_2Se_3$. Institut Laue-Langevin (2021), doi:10.5291/ILL-DATA.5-31-2837.

[17] J. Xu, Y. Xia, Z. Li, H. Chen, X. Wang, Z. Sun, and W. Yin, Multi-physics instrument: Total scattering neutron time-of-flight diffractometer at china spallation neutron source, Nucl. Instrum. Methods Phys. Res., Sect. A **1013**, 165642 (2021).

[18] See Supplemental Material at http://link.aps.org/supplemental/10.1103/PhysRevB.109.184428 for the details of the powder neutron diffractometers and refinements.

[19] J. Rodríguez-Carvajal, Recent advances in magnetic structure determination by neutron powder diffraction, Phys. B: Condens. Matter **192**, 55 (1993).

[20] W. Zheng, V. Balédent, M. B. Lepetit, P. Retailleau, E. V. Elslande, C. R. Pasquier, P. Auban-Senzier, A. Forget, D. Colson, and P. Foury-Leylekian, Room temperature polar structure and multiferroicity in $BaFe_2Se_3$, Phys. Rev. B **101**, 020101(R) (2020).

[21] M. J. Weseloh, V. Balédent, W. Zheng, M. Verseils, P. Roy, J. B. Brubach, D. Colson, A. Forget, P. Foury-Leylekian, and M.-B. Lepetit, Lattice dynamics of $BaFe_2Se_3$, J. Phys.: Condens. Matter **34**, 255402 (2022).

[22] I. Radelytskyi, P. Aleshkevych, D. Gawryluk, M. Berkowski, T. Zajarniuk, A. Szewczyk, M. Gutowska, L. Hawelek, P. Wlodarczyk, J. Fink-Finowicki *et al.*, Structural, magnetic, and magnetocaloric properties of $Fe_7Se_8$ single crystals, J. Appl. Phys. **124**, 143902 (2018).

[23] M. Mourigal, S. Wu, M. B. Stone, J. R. Neilson, J. M. Caron, T. M. McQueen, and C. L. Broholm, Block magnetic excitations in the orbitally selective Mott insulator $BaFe_2Se_3$, Phys. Rev. Lett. **115**, 047401 (2015).

[24] J. Gao, Y. Teng, W. Liu, S. Chen, W. Tong, M. Li, X. Zhao, and X. Liu, The synthesis and magnetic properties of $BaFe_2Se_3$ single crystals, RSC Adv. **7**, 30433 (2017).

[25] B. Saparov, S. Calder, B. Sipos, H. Cao, S. Chi, D. J. Singh, A. D. Christianson, M. D. Lumsden, and A. S. Sefat, Spin glass and semiconducting behavior in one-dimensional $BaFe_{2-\delta}Se_3(\delta \approx 0.2)$ crystals, Phys. Rev. B **84**, 245132 (2011).

[26] W. G. Zheng, V. Balédent, L. Bocher, A. Forget, D. Colson, and P. Foury-Leylekian, Origin of spin-glass-like magnetic anomaly in the superconducting and multiferroic spin ladder $BaFe_2Se_3$, Phys. Rev. B **107**, 024423 (2023).

[27] S. Imaizumi, T. Aoyama, R. Kimura, K. Sasaki, Y. Nambu, M. Avdeev, Y. Hirata, Y. Ikemoto, T. Moriwaki, Y. Imai, and K. Ohgushi, Structural, electrical, magnetic, and optical properties of iron-based ladder compounds $BaFe_2(S_{1-x}Se_x)_3$, Phys. Rev. B **102**, 035104 (2020).

[28] V. Svitlyk, G. Garbarino, A. Rosa, E. Pomjakushina, A. Krzton-Maziopa, K. Conder, M. Nunez-Regueiro, and M. Mezouar, High-pressure polymorphism of $BaFe_2Se_3$, J. Phys.: Condens. Matter **31**, 085401 (2019).

[29] A. Olariu, F. Rullier-Albenque, D. Colson, and A. Forget, Different effects of Ni and Co substitution on the transport properties of $BaFe_2As_2$, Phys. Rev. B **83**, 054518 (2011).

[30] V. Brouet, P.-H. Lin, Y. Texier, J. Bobroff, A. Taleb-Ibrahimi, P. Le Fèvre, F. Bertran, M. Casula, P. Werner, S. Biermann, F. Rullier-Albenque, A. Forget, and D. Colson, Large temperature dependence of the number of carriers in Co-doped $BaFe_2As_2$, Phys. Rev. Lett. **110**, 167002 (2013).

[31] J. Herbrych, J. Heverhagen, N. D. Patel, G. Alvarez, M. Daghofer, A. Moreo, and E. Dagotto, Novel magnetic block states in low-dimensional iron-based superconductors, Phys. Rev. Lett. **123**, 027203 (2019).

[32] Two extra electrons from the doping by Ni on the Fe site $\times 2$ from the chemical formula $\times x$.

[33] Following Herbrych *et al.*, there are $4 + 0.16$ electrons to fill three Fe orbitals (bands). One orbital (band) is strongly correlated and is filled by one electron. The 3.16 remaining electrons have to be distributed into two degenerated bands. thus $n = 2.58$.

[34] V. Balédent, F. Rullier-Albenque, D. Colson, G. Monaco, and J.-P. Rueff, Stability of the Fe electronic structure through temperature-, doping-, and pressure-induced transitions in the $BaFe_2As_2$ superconductors, Phys. Rev. B **86**, 235123 (2012).

[35] V. Balédent, F. Rullier-Albenque, D. Colson, J. M. Ablett, and J.-P. Rueff, Electronic properties of $BaFe_2As_2$ upon doping and pressure: The prominent role of the as *p* orbitals, Phys. Rev. Lett. **114**, 177001 (2015).